Thermal Stability in Evaporating Liquid Disks by Local Potential Technique

Nengli Zhang* and Zhihong Jiang*
Tsinghua University, Beijing, China
and
Wen-Jei Yang†
University of Michigan, Ann Arbor, Michigan

A nonequilibrium thermodynamical, local potential method (energy-stability theory) is employed to analyze thermal stability in an evaporating liquid disk that simulates a sessile drop with a planar free surface. Both buoyancy and thermocapillary instability mechanisms are taken into account. The neutral stability surface in Rayleigh–Marangoni wave-number coordinates is obtained by means of the supernormal mode analysis. The mechanism for the onset of Benard–Marangoni convection is disclosed. The effects of the disk radius-thickness ratio and Prandtl number on the stability are determined. The validity of the theoretical model is borne out by its agreement with experiments.

Nomenclature

A = coefficient as defined by Eq. (31); A^* steady-state component
a_1, a_2 = coefficients of A in Eqs. (44) and (45)
B = coefficient as defined by Eq. (30); B^* steady-state component
b = $(2 + Ev)/(1 + Ev)$
b_1, b_2 = coefficients of B in Eqs. (44) and (45)
D = differential operator, d/dZ
d = disk diameter, mm
Ev = evaporative perturbation number as defined by Eq. (18)
G = disk radius-thickness ratio = $d/2H$
g = gravitational acceleration, m/s^2
H = disk thickness, mm
h_{fg} = latent heat of vaporization, J/g
J_0 = Bessel function of zeroth order
J_1 = Bessel function of first order
k = thermal conductivity of disk, W/m·K
Ma = Marangoni number as defined by Eq. (18)
$\dot{m}$ = rate of evaporation, g/s
N^0, N^1 = integrals as defined by Eq. (36)
n = half-wave number
P = dimensionless liquid pressure as defined by Eq. (13a)
$\hat{P}$ = amplitude of P perturbation
Pr = Prandtl number as defined by Eq. (13c)
p = liquid pressure, Pa
$\bar{p}$ = liquid pressure at stationary state, Pa
p' = perturbation of p, Pa
R = r/H
Ra = Rayleigh number as defined by Eq. (13c)
r = radial coordinate, mm
S = solid-liquid interfacial area, m^2
T = liquid temperature, °C; also dimensionless quantity $T'/\Delta T$; T_b, solid-liquid interface; T_m, mean value; T_s, disk surface
$\hat{T}$ = amplitude of T perturbation; $\hat{T}^*$, function as defined by Eq. (37)
$\bar{T}$ = liquid temperature at stationary state, °C
T' = perturbation of T, °C
ΔT = $T_b - T_s$, °C
t = time, s
U = volume, mm^3
V = dimensionless perturbed velocity; V_r, r component; V_z, z component
$\hat{V}$ = dimensionless amplitude of velocity perturbation; $\hat{V}_r$, r component; $\hat{V}_z$, z component; $\hat{V}_z^*$, function as defined by Eq. (38)
v = liquid velocity, mm/s; v_r, r component; v_z, z component
$\bar{v}$ = liquid velocity at stationary state, mm/s; $\bar{v}_r$, r component; $\bar{v}_z$, z component
v' = perturbation of v, mm/s, v_r', r component; v_z', z component
Z = z/H
z = axial coordinate, mm
α = thermal diffusivity of liquid, mm^2/s
β = coefficient of thermal expansion, 1/K
λ_n = wave parameter as defined by Eq. (23)
μ_n = nth zero of J_1 function
ν = kinematic viscosity, mm^2/s
ρ = liquid density, Kg/m^3; ρ_m, mean value of T_m
σ = negative of the derivative of surface tension with respect to temperature, N/mm-K
τ = dimensionless time as defined by Eq. (13b)
Φ = dimensionless local potential; Φ^*, zeroth-order approximation
ω = amplification factor, 1/s

Superscripts

$\hat{}$ = perturbed state (of dimensionless quantity)
$'$ = perturbed state (of dimensional quantity)
$-$ = stationary (initial) state
$*$ = unperturbed state (zeroth-order approximation)

Subscripts

b = solid-liquid interface
m = average value

Received April 27, 1987; revision received Jan. 22, 1988.

*Associate Professor, Department of Thermal Engineering.
†Graduate Student, Department of Mechanical Engineering and Applied Mechanics.

n = half-wave number n
r = radial component
s = disk-free surface
z = axial component

Introduction

It is well known that fluid mechanical instabilities and convective transfer processes determine, to a large extent, heat and mass transport in both nature and technology. For example, the atmospheric structure of planets, the growth of flame, and solidification cells are determined largely by convective transfer processes and instabilities.[1]

When the adverse temperature gradient in a liquid layer on a flat plate exceeds a critical value, the liquid layer will undergo a change from a steady, conductive state into a cellular convective state. This thermal instability phenomenon was first observed by Thomson[2] in 1881. It was Benard who carried out an experimental study on the phenomena in 1900.[3] Kalinin proposed a method of modeling the code recording of signals in biological systems on the basis of Benard cell structure.[4]

What is the mechanism of cellular convection in a liquid layer? By theoretical analysis, Rayleigh[5] interpreted buoyancy force as the cause of such an instability. In 1958, Person's analysis[6] concluded surface-tension force induced the instability. However, Nield[7] later disclosed the combined action of buoyancy and surface-tension forces to be the cause. Buoyancy force dominates in a thick fluid layer, whereas surface-tension force controls instabilities in a thin layer. A large number of references have extended the studies to include the effects of various parameters and double diffusion (thermal and solutal) on instability phenomena and convective transport.

A new area of study concerns instability and convective problems in liquid drops' evaporation on a flat plate.[8] Unique to droplet systems is the importance of a surface-tension force that may surpass buoyancy force and becomes the dominant factor in instability and convection phenomena. This is especially true when the drop is in a reduced-gravity environment. Evaporation can induce disturbances at the drop surface, resulting in thermocapillary instability. Theoretical results obtained for a liquid layer cannot be applied to predict the instability in a liquid drop because of edge effects. Owing to the time-varying shape and complex geometry of liquid drops, instability analysis is mathematically intractable. Only a hemispherical model of drop geometry has been treated for buoyancy-induced instability[9] and buoyancy thermocapillary convection phenomena.[10] A liquid volume of hemispherical shape was found to be more stable than a liquid layer.[9] The region of zero streamline separating the buoyancy-induced flow regime from the surface tension-induced one was attributed to Benard cells that migrated from the edge to top of the drop with time.[10]

The methods of energy- and linear-stability theory complement each other in demarcating the region of parameter space, in which subcritical instabilities are allowable. The latter (for example, Refs. 7, 9, and 11) such as the Orr–Sommerfeld equation gives a sufficient condition for instability, whereas the former (for example, Refs. 12–14) provides a sufficient condition for stability. The energy theory involves the construction of a Lyapunov functional that carries the energy given to a disturbance at steady state whose stability is then studied.[12]

A function y is called a Lyapunov function if it possesses the properties of $y > 0$ and $\partial y/\partial t \leq 0$. The process described by a Lyapunov function is stable or asymptotically stable (if $\partial y/\partial t < 0$). This is the Lyapunov stability theory. The square of the distance at time t between the perturbed and steady-state trajectories in the phase space can be a Lyapunov function. Later, Glansdorff and Prigogine proposed using the second differential of specific entropy, d^2s, as a generalized Lyapunov function. If $d^2s < 0$ and $\partial/\partial t\ (d^2s) \geq 0$, the process is thermodynamically stable or asymptotically stable [in the case of $\partial/\partial t\ (d^2s) > 0$].

A more generalized Lyapunov function is defined as d^2z with

$$z = s - (1/2T_0)|\boldsymbol{v}|^2$$

Here, T_0 denotes the steady-state temperature and $|v|^2/2$ is the specific kinetic energy of the system. If $d^2z < 0$ and $\partial/\partial t\ (d^2z) \geq 0$, the process is thermodynamically as well as hydrodynamically stable or asymptotically stable [for $\partial/\partial t\ (d^2z) > 0$].

The energy method was first applied to investigate buoyancy surface-tension instability in a liquid layer heated from below.[13] It was extended to the case of a deformable free surface.[14]

Glansdorff and Prigogine defined an integral Φ as the local potential, whose magnitude is an absolute minimum at steady state and perturbation from steady state is positive

$$\delta\Phi = 0 \qquad \text{and} \qquad \Delta\Phi > 0$$

The first expression assures us that the integral is stationary in nature. The local potential can be used in conjunction with the self-consistent method of numerical analysis to determine stability; this is called the local potential technique. It leads to the same "computer-ready" eigenvalue problem as obtained by means of the Galerkin method or the variational method of Lee and Reynolds. When the same trial functions are employed, all three methods would yield the same numerical results and critical Reynolds number for instability with the same accuracy. They are all equivalent.[15] However, the local potential technique is preferable to the other two methods for the following reasons: 1) It does not introduce an adjoint problem. 2) In hydrodynamic stability problems, it requires only one type of approximating function for the unknown variables as compared with two types of approximating functions needed in the other two methods. 3) It uniquely possesses a minimum property (the local potential has an absolute minimum at steady state) that establishes a convergence criterion for the numerical technique. The first two merits simplify the computational procedure and reduce its time. In some sense, the local potential is a generalization of the concept of thermodynamic potentials. Details of the local potential technique for stability analysis are presented later.

In the present study, a sessile drop is simulated by a liquid disk. Experiments[8] have indicated that minute liquid drops being carefully placed on a solid plate exhibit the shape of a spherical segment, or so-called lens shape. For example, a drop of 8 to 10 ml in volume has a base diameter d of approximately 8 mm and a height h of about 0.3 to 0.4 mm on a plate. It should be noted that the diameter-to-height ratio is at least 20, being very flat. Such a drop may approximate a disk-shaped liquid having the same base diameter but has one-half the height. The approximation leads to an error less than 9% in a free surface area and practically the same volume for a liquid drop in the aforementioned range of volume, base diameter, and height. For a disk-shaped liquid with a diameter of 8 mm and a height of 0.15 to 2 mm, the side surface area is less than 10% of the total free surface area. Therefore, one may ignore the effect of side surface in the interest of simplifying mathematical manipulation such that the exact solution of the problem may be obtained. Otherwise, one would be faced with a nonlinear analysis resulting in numerical computation. It should be noted that the case considered actually is that of an evaporating liquid contained in a disk container with slippery side walls. The case is of some interest by itself.

The theoretical model for a liquid disk is different from that for a liquid layer. Although normal mode analysis is employed in the latter case, supernormal mode analysis is applied to the disk because the perturbation equations for fluid flow and heat transfer have no normal solutions.

The present work presents a theoretical analysis of buoyancy and thermocapillary-induced stability in liquid disks evaporating on a flat plate. The system geometry simulates flat-top liquid drops. A drop of unstable evaporating-type liquids has a planar free surface at certain time period during its evaporation process.[8] A thermally nonequilibrium, local potential method is employed to determine stability limits for the free surface flow. The validity of the theoretical analysis is borne out by its agreement with experimental observations.

Theory

A. Local Potential Technique

The variational formulation that follows next is the local potential method. It begins with the derivation of the linearized equations for transport phenomena in the perturbed state. The same procedure for elimination of variables is performed as that done in deriving the Orr–Sommerfeld equation for hydrodynamic instability. The resulting expression is then integrated over the control volume, with the appropriate boundary conditions incorporated. An integral in the final expression is selected as the local potential Φ such that the Euler–Lagrange equation of the functional (i.e., the integral) and the a posteriori subsidiary conditions restore the perturbed balance equations. One must observe that for any arbitrary increment in the perturbed variable, the resulting change in the local potential $\Delta\Phi$ is strictly positive. Hence, according to the Glansdorff–Prigogine theory, the initial value (at zero time) of the local potential is an absolute minimum. The absolute minimum property of Φ may be utilized in evaluating all the unknown variables contained in the local potential by numerical analysis.

In the numerical method that immediately follows the construction of the local potential, each unknown variable is expanded into a series consisting of trial functions f_i and their coefficients a_i. The trial functions must satisfy the appropriate boundary conditions. One should bear in mind that the number of variational parameters increases with the number of unknown variables to be determined and that the computational effort increased accordingly. On the substitution of the approximating functions into the local potential, the Rayleigh–Ritz method ($\partial\Phi/\partial a_i = 0$) is applied. It yields a system of linear homogeneous equations in the a_i. For the nontrivial solutions to exist, the determinant of the coefficients of the a_i must be zero. The characteristic determinant thus derived establishes an eigenvalue problem.

B. Formulation of the Problem

Consider a liquid disk, simulating a drop with a planar interface, being placed on flat plate, as shown in Fig. 1. It has a diameter d and a height H. Let T_s and T_b be the temperature of the disk surface and the solid-liquid interface, respectively. The liquid is assumed to be Newtonian in type with constant physical properties except density in the buoyancy term of the momentum equation. There is no temperature and velocity perturbation at the solid-liquid interface. The viscous heating effect is neglected. Then, both the velocity and temperature fields in the disk are two-dimensional and governed by the following equations in cylindrical coordinates (r,z,θ):

$$\frac{\partial v_r}{\partial \gamma} + \frac{v_r}{\gamma} + \frac{\partial v_z}{\partial z} = 0 \tag{1}$$

Momentum equations:

$$\frac{\partial v_r}{\partial t} + v_r\frac{\partial v_r}{\partial r} + v_z\frac{\partial v_r}{\partial z} = -\frac{1}{\rho_m}\frac{\partial p}{\partial r} + \nu\left(\nabla^2 v_r - \frac{v_r}{r^2}\right) \tag{2}$$

$$\frac{\partial v_z}{\partial t} + v_r\frac{\partial v_z}{\partial r} + v_z\frac{\partial v_z}{\partial z} = -\frac{1}{\rho_m}\frac{\partial p}{\partial z} - \frac{\rho}{\rho_m}g + \nu\nabla^2 v_z \tag{3}$$

Heat equation:

$$\frac{\partial T}{\partial t} + v_r\frac{\partial T}{\partial r} + v_z\frac{\partial T}{\partial z} = \alpha\nabla^2 T \tag{4}$$

where

$$\nabla^2 = \frac{1}{r}\frac{\partial}{\partial r}\left(r\frac{\partial}{\partial r}\right) + \frac{\partial^2}{\partial z^2} \tag{5}$$

Consider a disk in which a steady-state, adverse temperature gradient is maintained. Let there be no motion. The basic (initial) state is then described by

$$\bar{v}_r = \bar{v}_z = 0 \tag{6a}$$

$$\frac{\partial \bar{p}}{\partial r} = 0 \tag{6b}$$

$$\frac{\partial \bar{p}}{\partial z} = -\bar{\rho}g \tag{7}$$

$$\nabla^2\bar{T} = 0 \tag{8}$$

Subject to the boundary conditions

$$\bar{T} = T_b \quad \text{at} \quad z = 0; \qquad \bar{T} = T_s \quad \text{at} \quad z = H$$

the solution of Eq. (8) appropriate to the disk is

$$\bar{T} = T_b - \frac{\Delta T}{H}z \tag{6c}$$

in view of $\partial\bar{T}/\partial r = 0$. Since

$$\bar{\rho} = \rho_m[1 - \beta(\bar{T} - T_m)] \tag{6d}$$

Equation (7) is integrated to give

$$\bar{p} = -\rho_m g z + \rho_m g\beta(T_b - T_m)z - \tfrac{1}{2}\rho_m g\beta(\Delta T z^2/H) \tag{6e}$$

Let the initial state described by Eq. (6) be slightly perturbed. Let v_r', v_z', p', and T' denote, respectively, the velocity components, pressure, and temperature in the perturbed state. The problem is considered on the basis of Boussinesq's approximation. By ignoring terms of the second and higher orders in the perturbations, Eqs. (1–4) yield the disturbance equations in dimensionless form as

$$\frac{\partial V_r}{\partial R} + \frac{V_r}{R} + \frac{\partial V_z}{\partial Z} = 0 \tag{9}$$

$$\frac{\partial V_r}{\partial \tau} = -\frac{\partial P}{\partial R} + \nabla^2 V_r - \frac{V_r}{R^2} \tag{10}$$

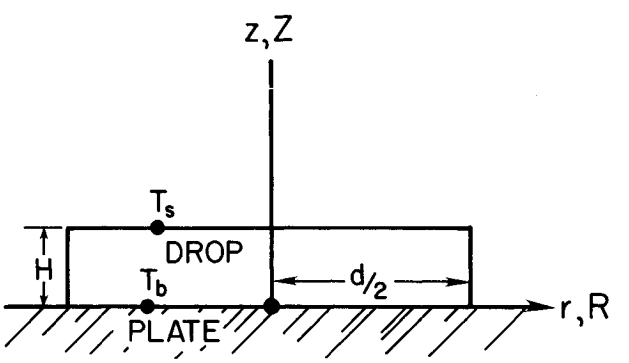

Fig. 1 Physical model of an evaporating liquid disk on a plate.

$$\frac{\partial V_z}{\partial \tau} = -\frac{\partial P}{\partial Z} + RaT + \nabla^2 V_z \tag{11}$$

$$Pr\frac{\partial T}{\partial \tau} = V_z + \nabla^2 T \tag{12}$$

Here,

$$V_r = \frac{v_r' H}{\alpha};\quad V_z = \frac{v_z' H}{\alpha};\quad P = \frac{p'}{\rho_m}\frac{H^2}{v\alpha};\quad T = \frac{T'}{\Delta T} \tag{13a}$$

$$R = \frac{r}{H};\quad Z = \frac{z}{H};\quad \tau = \frac{vt}{H^2} \tag{13b}$$

$$Pr = \frac{v}{\alpha};\quad Ra = \frac{g\beta H^3 \Delta T}{\alpha v} \tag{13c}$$

Pr and *Ra* are the Prandtl and Rayleigh numbers, respectively.

The boundary conditions in dimensionless form are at $Z = 1$,

$$V_z = 0 \tag{14a}$$

$$\frac{\partial T}{\partial Z} = -Ev\,T \tag{14b}$$

$$\frac{\partial V_r}{\partial Z} + \frac{\partial V_z}{\partial R} = -Ma\frac{\partial T}{\partial R} \tag{14c}$$

at $Z = 0$,

$$V_r = V_z = T = 0 \tag{15}$$

at $R = G$,

$$V_r = 0 \tag{16a}$$

$$V_z \quad \text{and} \quad T \text{ are limited functions} \tag{16b}$$

at $R = 0$,

$$\frac{\partial V_z}{\partial R} = \frac{\partial T}{\partial R} = 0 \quad \text{and} \quad V_r \text{ is a limited function} \tag{17}$$

in which

$$Ev = \frac{\dot{m}' h_{fg} H}{kST_s'};\quad Ma = \frac{\sigma H \Delta T}{\alpha \rho_m v};\quad G = \frac{d}{2H} \tag{18}$$

The evaporative perturbation and Marangoni numbers, are *Ev* and *Ma*, respectively, whereas *G* denotes the radius-height ratio of the disk. It is obvious that the flow and temperature fields are coupled through Eqs. (11), (12), and (14c).

The Bessel function of order 1, $J_1[\mu_n R/G]$, for $n = 1,2,...$ forms a complete set of orthogonal functions in the interval $(0, G)$. μ_n is its nth zero. The boundary conditions for the perturbed velocity V_r at $R = 0$ and G are the same characteristics of $J_1[\mu_n R/G]$ and for V_z they are the same as those of $J_0[\mu_n R/G]$. Hence, in order to analyze the disturbance in supernormal modes, one writes the perturbations as

$$V_r = \hat{V}_r(Z) J_1(\sqrt{\lambda_n} R)\exp(-\omega t) \tag{19}$$

$$V_z = \hat{V}_z(Z) J_0(\sqrt{\lambda_n} R)\exp(-\omega t) \tag{20}$$

$$T = \hat{T}(Z) J_0(\sqrt{\lambda_n} R)\exp(-\omega t) \tag{21}$$

$$P = \hat{P}(Z) J_0(\sqrt{\lambda_n} R)\exp(-\omega t) \tag{22}$$

where

$$\lambda_n = [\mu_n/G]^2 \tag{23}$$

ω is the amplification factor that determines the degree of amplification or damping. It is a real number, implying that the principle of the exchange of stabilities is valid. λ_n is the wave parameter of the disturbance and the quantity with the superscript ˆ a dimensionless amplitude (i.e., eigenfunction). The continuity equation (9) is satisfied because

$$\hat{V}_r(Z) = -\hat{D}V_z(Z)/\sqrt{\lambda_n} \tag{24}$$

in which $D = \mathrm{d}/\mathrm{d}Z$. The substitution of Eqs. (19–22) into Eqs. (10–12) yields

$$\lambda_n \hat{P} = (D^2 - \lambda_n + \omega)D\hat{V}_z \tag{25}$$

$$D\hat{P} = (D^2 - \lambda_n + \omega)\hat{V}_z + Ra\hat{T} \tag{26}$$

$$\hat{V}_z + (D^2 - \lambda_n + \omega Pr)\hat{T} = 0 \tag{27}$$

They are subject to the boundary conditions, from Eqs. (14) and (15).

$Z = 1$:

$$\hat{V}_z = 0 \tag{28a}$$

$$D\hat{T} + Ev\hat{T} = 0 \tag{28b}$$

$$D^2\hat{V}_z = -\lambda_n Ma\hat{T} \tag{28c}$$

$Z = 0$:

$$\hat{V}_z = 0 \tag{29a}$$

$$D\hat{V}_z = 0 \tag{29b}$$

$$\hat{T} = 0 \tag{29c}$$

The boundary conditions at $R = 0$ and G are automatically satisfied. Since $\hat{P}$ can be eliminated by combining Eqs. (25) and (26), no boundary conditions are needed.

The perturbation amplitudes $\hat{T}$ and $\hat{V}_z$ may take the following forms that satisfy the boundary conditions (28) and (29):

$$\hat{T} = \sum_{i=1}^{N} a_i z^{i-1} \tag{30}$$

$$\hat{V}_z = \sum_{j=1}^{M} b_j z^{j-1} \tag{31a}$$

$$= Af(z) + Bg(z) \tag{31b}$$

in which a_i and b_j denote the coefficients, and A and B are the variational parameters. For $N = 3$, Eq. (29c) leads to $a_1 = 0$, whereas Eq. (28b) yields $a_2 = -ba_3$ where $b = (2 + Ev)/(1 + Ev)$. Hence, Eq. (30) becomes

$$\hat{T} = a_3 z(z - b) \tag{32}$$

Equations (28c), (31b), and (32) are combined to give

$$A\left(\frac{\mathrm{d}^2 f}{\mathrm{d}z^2}\right)_{z=1} + B\left(\frac{\mathrm{d}^2 g}{\mathrm{d}z^2}\right)_{z=1} = \lambda_n Ma\, a_3(b - 1) \tag{33}$$

Let

$$f(z) = z^2(z - 1)(2z - p) \tag{34}$$

$$g(z) = qz^2(z - 1) \tag{35}$$

where p and q are constants to be determined. The substitution of Eqs. (34) and (35) into Eq. (33) gives

$$p = 3;\quad q = \lambda_n Ma(b - 1)/4;\quad B = a_3 \tag{36}$$

Equations (31b) and (34–36) are combined to yield

$$\hat{V}_z = AZ^2(Z-1)(2Z-3) + B\frac{\lambda_n Ma}{4}(b-1)Z^2(Z-1) \quad (37)$$

which corresponds to Eq. (31a) with $M = 5$.

Let the quantity Φ be the local potential given to an arbitrary disturbance at a steady state whose stability is to be studied. Its differential is defined as

$$d\Phi = \Phi - \Phi^* = -\frac{1}{2}\int_U \frac{\partial}{\partial t}[(dV_r)^2 + (dV_z)^2 + (dT)^2]\, dU \quad (38)$$

Equations (10–12) are multiplied by $-dV_r$, $-dV_z$, and $-dT$, respectively, followed by integrating each equation over the entire drop volume. The resulting equations are summed up together. Applying the relationship

$$-\frac{\partial\phi}{\partial t}d\phi = -\frac{\partial}{\partial t}(\phi^* + d\phi)\, d\phi = -\frac{1}{2}\frac{\partial}{\partial t}(d\phi)^2 - \frac{\partial\phi^*}{\partial t}d\phi \quad (39)$$

and the fractional integral of Z, one obtains

$$\begin{aligned}\Phi = \int_U \Bigg\{ &\left[\frac{\partial V_r^*}{\partial t} + \frac{\partial p^*}{\partial r} - \frac{1}{r}\frac{\partial}{\partial r}\left(r\frac{\partial V_r^*}{\partial r}\right) + \frac{V_r^*}{r^2}\right]V_r \\ &+ \left[\frac{\partial V_z^*}{\partial t} - RaT^* - \frac{1}{r}\frac{\partial}{\partial r}\left(r\frac{\partial V_z^*}{\partial r}\right)\right]V_z \\ &+ \left[\frac{\partial T^*}{\partial t} - \frac{1}{Pr}V_r^* - \frac{1}{Pr}\frac{1}{r}\frac{\partial}{\partial r}\left(r\frac{\partial T^*}{\partial r}\right)\right]T \\ &+ \frac{1}{2}\left(\frac{\partial V_r}{\partial Z}\right)^2 - P^*\frac{\partial V_z}{\partial Z} + \frac{1}{2}\left(\frac{\partial V_z}{\partial Z}\right)^2 + \frac{1}{2Pr}\left(\frac{\partial T}{\partial Z}\right)^2\Bigg\} dU \\ &+ \int_0^G r\, dr\left(-\frac{\partial V_r^*}{\partial Z}V_r + P^*V_z - \frac{\partial V_z^*}{\partial Z}V_z - \frac{1}{Pr}\frac{\partial T^*}{\partial Z}T\right)_{z=0}^{z=1}\end{aligned} \quad (40)$$

It can be shown that the consequent Euler–Lagrange equation of the foregoing expression is the characteristic equation.

Equations (19–22) and the associated boundary conditions (28) and (29) are substituted into Eq. (40) whose terms involving $\hat{P}$ are eliminated by the substitution of Eq. (25). With rearrangements, it yields

$$\begin{aligned}\Phi = &\exp(-2\omega t)N^1\int_0^1\left[\frac{1}{\lambda_n}D^3\hat{V}_z^*D\hat{V}_z + \frac{1}{2\lambda_n}(D\hat{V}_z)^2\right]dZ \\ &+ \exp(-2\omega t)N^0\int_0^1\Bigg[(\lambda_n-\omega)\hat{V}_z^*\hat{V}_z - \frac{1}{\lambda_n}D^3\hat{V}_z^*D\hat{V}_z \\ &+ \frac{1}{\lambda_n}(\lambda_n-\omega)D\hat{V}_z^*D\hat{V}_z - Ra\hat{T}^*\hat{V}_z + \frac{1}{2}(D\hat{V}_z)^2 \\ &+ \left(\frac{\lambda_n}{Pr}-\omega\right)\hat{T}^*\hat{T} - \frac{1}{Pr}\hat{V}_z^*\hat{T} + \frac{1}{2Pr}(D\hat{T})^2\Bigg]dZ \\ &+ \exp(-2\omega t)N^0\left(-D\hat{V}_r^*\hat{V}_r - \frac{1}{Pr}D\hat{T}^*\hat{T}\right)_{z=1}\end{aligned} \quad (41)$$

Here, the norms of $J_1(\sqrt{\lambda_n}r)$ and $J_0(\sqrt{\lambda_n}r)$ are, respectively,

$$N^1 = \int_0^G [J_1(\sqrt{\lambda_n}r)]^2 r\, dr; \quad N^0 = \int_0^G [J_0(\sqrt{\lambda_n}r)]^2 r\, dr \quad (42)$$

Since

$$\hat{T}^* = B^*Z(Z-b) \quad (43)$$

$$\hat{V}_z^* = A^*Z^2(Z-1)(2Z-3) + B^*\frac{\lambda_n Ma}{4}(b-1)Z^2(Z-1) \quad (44)$$

Substituting Eqs. (32), (37), (43), and (44) into Eq. (39) followed by rearrangements, one gets

$$\begin{aligned}\Phi = &\exp(-2\omega t)A^*A\left[-\frac{36N}{5\lambda_n} + \frac{19}{630}(\lambda_n-\omega)N^0\right. \\ &\left. + \frac{36N^0}{5\lambda_n} + \frac{24}{70}\frac{1}{\lambda_n}(\lambda_n-\omega)N^0\right] \\ &+ \exp(-2\omega t)A^*B\Bigg[(b-1)MaN^1 \\ &- \frac{1}{240}\lambda_n(\lambda_n-\omega)(b-1)MaN^0 - (b-1)MaN^0 \\ &- \frac{1}{20}(\lambda_n-\omega)(b-1)MaN^0 - \left(\frac{11}{210}-\frac{b}{12}\right)\frac{1}{Pr}N^0\Bigg] \\ &+ \exp(-2\omega t)B^*A\Bigg[-\frac{1}{240}\lambda_n(\lambda_n-\omega)(b-1)MaN^0 \\ &- \frac{1}{20}(\lambda_n-\omega)(b-1)MaN^0 - \left(\frac{11}{210}-\frac{b}{12}\right)RaN^0 \\ &+ (b-1)MaN^0\Bigg] + e^{-2\omega t}B^*B \\ &\times\Bigg[\frac{1}{1680}\lambda_n^2(\lambda_n-\omega)(b-1)^2Ma^2N^0 \\ &+ \frac{1}{120}\lambda_n(\lambda_n-\omega)\cdot(b-1)^2Ma^2N^0 + \lambda_n\left(\frac{1}{120}-\frac{b}{80}\right) \\ &\times(b-1)MaRaN^0 - \left(\frac{1}{5}-\frac{b}{2}+\frac{b^2}{3}\right)\left(\frac{\lambda_n}{Pr}-\omega\right)N^0 \\ &+ \lambda_n\left(\frac{1}{120}-\frac{b}{80}\right)(b-1)\frac{Ma}{Pr}N^0 - \frac{1}{4}\lambda_n(b-1)^2Ma^2N^0 \\ &- (2-3b+b^2)\frac{N^0}{Pr}\Bigg] + \exp(-2\omega t)A^2\left(\frac{6}{35}N^0 + \frac{6N^1}{35\lambda_n}\right) \\ &+ \exp(-2\omega t)AB\left[-\frac{1}{20}(b-1)MaN^1 - \frac{\lambda_n}{20}(b-1)MaN^0\right] \\ &+ \exp(-2\omega t)B^2\Bigg[\frac{\lambda_n}{240}(b-1)^2Ma^2N^1 \\ &+ \frac{1}{240}\lambda_n^2(b-1)^2Ma^2N^0 + \left(\frac{2}{3}-b+\frac{b^2}{2}\right)\frac{N^0}{Pr}\Bigg]\end{aligned} \quad (45)$$

If a steady flow is produced inside the disk after disturbance, then Φ must take a minimum value. Hence,

$$\frac{\partial\Phi}{\partial A} = \frac{\partial\Phi}{\partial B} = 0 \quad (46)$$

Equation (45) is differentiated with respect to A and B separately followed by the applications of Eq. (46) and the auxiliary conditions[14]

$$A^* = A \quad (47a)$$

$$B^* = B \quad (47b)$$

It produces

$$A\left[-\frac{36}{5\lambda_n}N^1+\frac{19}{630}(\lambda_n-\omega)N^0+\frac{36}{5\lambda_n}N^0+\frac{24}{70\lambda_n}(2N^0-\omega N^0+N^1)\right]+B\left[-\frac{\lambda_n}{240}(\lambda_n-\omega)(b-1)MaN^0-\frac{1}{20}(\lambda_n-\omega)(b-1)MaN^0-\left(\frac{11}{210}-\frac{b}{12}\right)RaN^0+(b-1)MaN^0-\frac{(b-1)}{20}MaN^1-\frac{\lambda_n}{20}(b-1)MaN^0\right]=0 \tag{48}$$

$$A\left[(b-1)MaN^1-\frac{\lambda_n}{240}(\lambda_n-\omega)(b-1)MaN^0-(b-1)MaN^0-\frac{1}{20}(\lambda_n-\omega)(b-1)MaN^0-\left(\frac{11}{210}-\frac{b}{12}\right)\frac{N^0}{Pr}-\frac{1}{20}(b-1)MaN^1-\frac{\lambda_n}{20}(b-1)MaN^0\right]+B\left[\frac{\lambda_n^2}{1680}(\lambda_n-\omega)\times(b-1)^2Ma^2N^0+\frac{\lambda_n}{120}(\lambda_n-\omega)(b-1)^2Ma^2N^0+\lambda_n\left(\frac{1}{120}-\frac{b}{80}\right)(b-1)MaRaN^0-\left(\frac{1}{5}-\frac{b}{2}+\frac{b^2}{3}\right)\times\left(\frac{\lambda_n}{Pr}-\omega\right)N^0+\lambda_n\left(\frac{1}{120}-\frac{b}{80}\right)(b-1)\frac{Ma}{Pr}N^0-\frac{\lambda_n}{4}(b-1)^2Ma^2N^0-(2-3b+b^2)\frac{N^0}{Pr}+\frac{\lambda_n}{120}(b-1)^2Ma^2N^1+\frac{\lambda_n^2}{120}(b-1)^2Ma^2N^0+\left(\frac{4}{3}-2b+b^2\right)\frac{N^0}{Pr}\right]=0 \tag{49}$$

Denoting the coefficients of A and B in Eqs. (48) and (49) as a_1, a_2 and b_1, b_2, respectively, Eqs. (48) and (49) can be rewritten as

$$a_1A+b_1B=0 \tag{50}$$

$$a_2A+b_2B=0 \tag{51}$$

Even though very small, the perturbations on the disk cannot be all zero. Therefore, A and B ($=a_3$) in Eqs. (32) and (37) cannot be all zero. This implies that the determinant of the homogeneous equations (50) and (51) must be zero, which means

$$a_1b_2+a_2b_1=0 \tag{52}$$

This is the characteristic equation of the disturbance that contains six parameters pertinent to instability, i.e., ω, λ_n, Pr, Ra, Ma, and Ev. The sign of ω determines whether the disturbance wave is amplified ($\omega>0$) or damped ($\omega<0$). For $\omega<0$, the disk is stable for the given value of wave parameter λ_n, whereas $\omega>0$ denotes instability. The limiting case $\omega=0$ corresponds to neutral (indifferent) disturbances, i.e., the limit of stability. The variation of b ranges from 1 to 2 for the evaporative perturbation number between zero and infinity. Therefore, b may be considered a fixed value, that is, $b=2$. For neutral stability ($\omega=0$), Eq. (52) is reduced to

$$\begin{aligned}Ra=[&M_1(0.004286\lambda_n^2Ma^2+0.12\lambda_nMa^2-3.84Pr^{-1}-0.12MaPr^{-1}-0.004167Ma^2\\&+0.06M_6Ma^2+9.6Pr^{-1}\lambda_n^{-1})+M_3(0.0000006\lambda_n^2+0.0000775\lambda_n-0.01608Pr^{-1}Ma^{-2}\\&+0.0000265Pr^{-1}Ma^{-1}-0.006111+0.0040013M_6-0.17143\lambda_n^{-1})+0.0525(N^1Ma)^2+(N^0Ma)^2\\&+M_4(0.9545-0.3657\lambda_n-0.1143Ma-0.001829\lambda_nMa)+M_5(0.095714\lambda_nMa+0.005714Pr^{-1}-1.05Ma\\&+0.05)]/(0.12M_1Ma+0.0000265M_3Ma^{-1}+0.1143M_2Ma-0.005714M_5+0.01319M_4)\end{aligned} \tag{53}$$

where

$$M_1=N^0(N^0-20N^1/21);\quad M_2=N^0(N^1-N^0)$$

$$M_3=(N^0\lambda_nMa)^2;\quad M_4=(N^0)^2/Pr$$

$$M_5=N^0N^1Ma;\quad M_6=N^1/N^0$$

Results and Discussion

The accuracy of the solutions for $\hat{T}$ and $\hat{V}_z$ depends on the values of M and N selected, whereas the resulting truncation errors are irrelevant to lower bounds on stability for finite disturbances. An increase in the values of N and M improves the accuracy of the solutions, but also causes an increase in the number of variational parameters that would require more computational effect. The reason for selecting $N=3$ and $M=5$ is to obtain the minimum number of variational parameters, which is 2 (namely, A and B). These values of N and M are large enough to give sufficient accuracy in $\hat{T}$ and $\hat{V}_z$.

A digital computer was used to calculate Eq. (53) for the critical Ra. Some representative results are presented in Figs. 2 and 3.

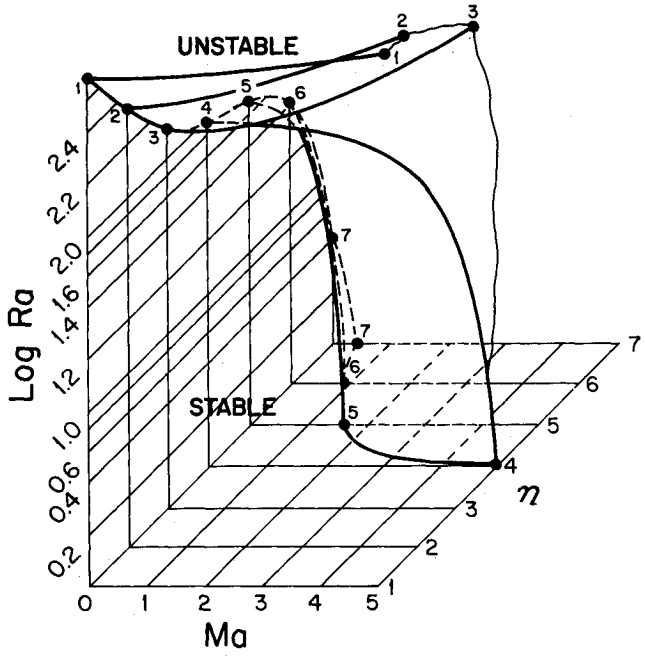

Fig. 2 Neutral stability surface in *Ra-Ma-n* coordinates for acetone disks with $Pr=5.4509$ and $G=15$.

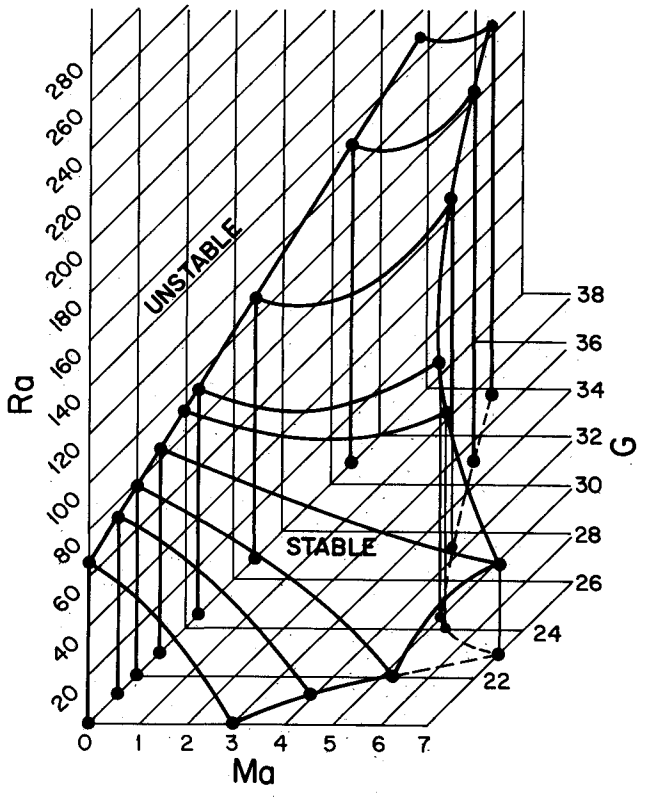

Fig. 3 Neutral stability surface in *Ra-Ma-G* coordinates for acetone disks with $Pr = 3.7370$ and $n = 6$.

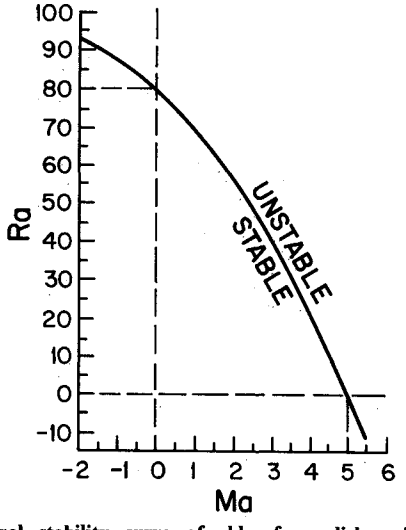

Fig. 4 Neutral stability curve of chloroform disks with $G = 15$, $Pr = 5.4509$, and $n = 4$.

Figure 2 depicts the neutral stability surface for chloroform disks with 6.0-mm diam, 0.2-mm height, and $Pr = 5.451$. It consists of the *Ra*, *Ma*, and *n* axes. Every point on the surface corresponds to $\omega = 0$, which separates the region of stable disturbances from that of unstable ones. The point has the smallest Rayleigh number below which all individual oscillations decay, whereas above that value at least some are amplified. This smallest *Ra* is the critical Rayleigh number or limit of stability for the *n*th mode. The half-wave number is *n*, corresponding to the aforementioned wave parameter λ_n. *n* represents the number of zeros of V_r, excluding that at $R = 0$. Figure 2 indicates $n = 7$ is the lowest neutral stability curve. All values of *Ra* for $n = 8$ are negative, which are physically meaningless. It should be noted that even for $n = 7$ or larger,

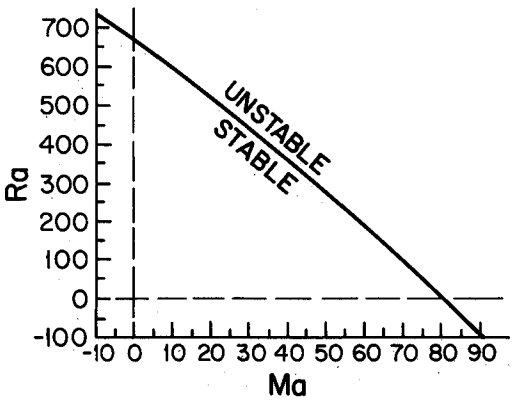

Fig. 5 Neutral stability curve of liquid layer for $n = 4$ and independent of *Pr*.[7]

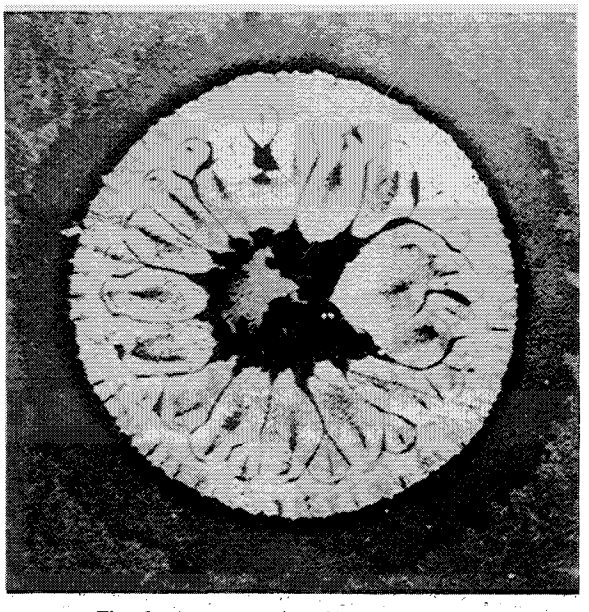

Fig. 6 An evaporating chloroform drop.

there is a range of negative *Ra*. It is therefore concluded that $n = 7$ is the most unstable mode. Different values of *G* and *Pr* would have a different neutral stability surface and, consequently, different values of *n* for the least curve. However, an increase in *Pr* would enhance the stability, but its effect is rather minor so it is not shown.

Figure 3 depicts the neutral stability surface of acetone drops with $Pr = 3.737$ and $n = 6$. It consists of the *Ra*, *Ma*, and *G* axes. For the value of *G* less than 22, the neutral stability surface concaves downward to intersect with the *Ma-G* plane. However, when *G* exceeds 22, the surface concaves upward, without cutting the *Ma-G* plane. The value of *Ra* increases with an increase in the radius-height ratio *G* for certain values of *Ma*. In general, an increase in *G* or a lowering of the gravitational center of a disk tends to enhance the stability. The evaporation of a very thin disk would not induce internal flow motion, because the radius-to-height ratio is too large. This disclosure has an important application in drop combustion on a hot wall. A fine drop would form a more thermally stable liquid volume on the wall than a larger drop.

It is seen in both Figs. 2 and 3 that the thermal stability of a liquid disk, or a disk-shaped drop, is determined by the interaction of *Ra* and *Ma*: When a critical state is reached by heating the plate or increasing surface evaporation, internal flow is induced by the disturbances of both surface-tension and buoyancy forces. This observation is in agreement with Nield's[7] for a large liquid volume.

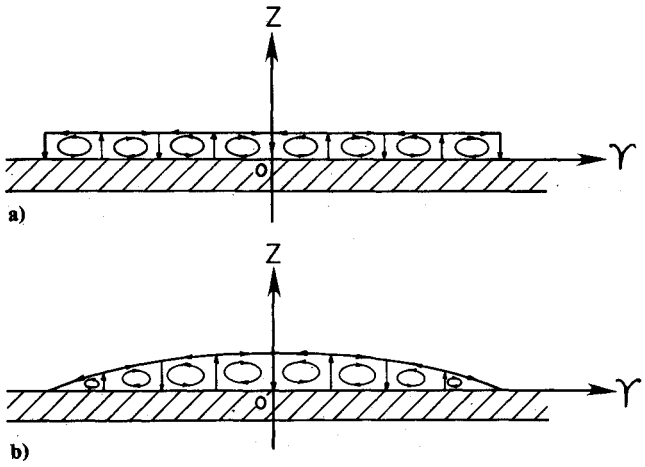

Fig. 7 A comparison of flow patterns obtained by present theory and experiment[16]: a) theoretical prediction for $n = 4$, and b) experimental result for $n = 4$.

It is of interest to compare the neutral stability of a liquid disk, Fig. 4, with that of a liquid layer, Fig. 5. Figure 4 is the neutral stability curve of chloroform ($CHCl_3$) with $G = 15$ and $Pr = 5.4509$, whereas Fig. 5 is that of a layer of any liquid with the wave number of 2.[1] When the half-wave number of the disturbance $n = 4$, two complete velocity waves are produced within the disk in the radial range between 0 and G. This means the wave number inside the disk is 2 (this wave number is the entire radial length divided by unit wavelength) in Fig. 4. A comparison of Figs. 4 and 5 reveals that at a stationary state, instability is more easily provoked in a disk shape than a liquid layer of the same wave number. In other words, the disk is more unstable than the liquid layer. In a disk, $(Ma, Ra) = (5, 0)$ can induce convection motion with the wave number of 2, whereas $(Ma, Ra) = (80, 0)$ is needed to cause convective motion in a layer with the same wave number. In reality, a drop on a plate has a certain curvature at the free surface and is thus more unstable than the theoretical prediction.

Comparison Between Theory and Experiment

In order to experimentally observe thermocapillary stability inside a drop that is simulated by a liquid disk, an experiment was conducted on an evaporation chloroform drop by means of flow visualization and optical photography.[16,17] A typical photo is presented in Fig. 6. Evaporation deprives the latent heat from the free surface, producing ΔT in the axial (vertical) direction.

Heat balance gives

$$\Delta T = \frac{\dot{m} h_{fg} H}{kS} \tag{54}$$

If we substitute Eq. (54) into Eqs. (13c) and (18), Ma and Ra for an evaporation drop can be evaluated.

The half-wave number n is found to be 4 from the cellular motion in Fig. 6. Hence, the neutral stability curve in Fig. 4 applies. Figure 4 predicts that when instability occurs, the convective motion shown in Fig. 7a would appear. Experimentally determined cellular convection in Fig. 6 (top view) is described in Fig. 7b (side view). A comparison of Figs. 7a and 7b indicates that the convective pattern in the chloroform drop after the disturbance of stationary state is verified by the experimental evidence. An experiment was also conducted on a water drop within which disturbances failed to induce fluid motion. The reason was that under the experimental conditions, the evaporation rate of water drop was not high enough to reach the limit of stability.

Conclusions

The local potential method is employed to determine the mechanism for inducing Benard cellular convection in a disk evaporating on a plate. The liquid disk simulates a sessile drop. The analysis with computational results indicates that both the Marangoni and Rayleigh numbers are related to the induction of convection in a disk. This observation is in agreement with the mechanism of instability in a liquid layer analyzed by Nield for a large liquid volume. A disk-type drop is found to be less stable than a liquid layer for the same wave number, however.

The mathematical model yields the neutral stability surface and curve. It is disclosed that an increase in the disk radius-height ratio enhances the stability at a stationary state. A disk of a higher Prandtl number is more stable than that of a smaller one but the effect of the Prandtl number on thermal stability is minor. The neutral stability curves for different wave numbers are compared.

Theoretical prediction agrees well with experimental results on the Benard cellular convection in an evaporating chloroform drop. Thus, the validity of the theory is proved, indicating the successful use of the local potential method for stability analysis.

References

[1]Zierep, J. and Oertel, H., Jr. (eds.), *Convective Transport and Instability Phenomena*, G. Braun, Karlsruhe, FRG, 1982.

[2]Thomson, J., "On a Changing Tessellated Structures in Certain Liquids," *Proceedings of the Glasgow Philosophical Society*, Vol. 13, 1882, p. 469.

[3]Benard, H., "Les Tourbillions Cellulaires dans une Nappe Liquide," *Revue Generale des Sciences*, Vol. 12, 1900, pp. 1261–1271, 1309–1328.

[4]Kalnin, A. A., "Possibility of the Distributed Code Recording of Signals in Non-Equilibrium Cooperative Systems (Structural Reflexia), *Biofizika*, Vol. 29, 1984, 117–121.

[5]Rayleigh, Lord, "On Convective Currents in a Horizontal Layer of Fluid, When the Higher Temperature is on the Under Side," *Philosophical Magazine*, Vol. 32, No. 192, 1916, pp. 529–547.

[6]Pearson, J. R. A., "On Convective Cells Induced by Surface Tension," *Journal of Fluid Mechanics*, Vol. 4, Part 5, 1958, pp. 489–500.

[7]Nield, D. A., "Surface Tension and Buoyancy Effects in Cellular Convection," *Journal of Fluid Mechanics*, Vol. 19, Part 3, 1964, pp. 341–352.

[8]Zhang, N. and Yang, W.-J., "Natural Convection in Evaporating Minute Drops," *Journal of Heat Transfer*, Vol. 104, No. 4, 1982, pp. 656–662.

[9]Han, J. C. and Yang, W.-J., "Thermal Instability in Liquid Droplets on a Heated Surface," *Journal of Heat Transfer*, Vol. 102, No. 5, 1980, pp. 581–583.

[10]Duh, J. C., "Thermocapillary-Buoyancy Convection in Drop-Shaped System by Phase Change," Ph.D. Thesis, Dept. of Mechanical Engineering and Applied Mechanics, the University of Michigan, Ann Arbor, MI, 1987.

[11]Chandrasekhar, S., *Hydrodynamic and Hydromagnetic Stability*, Oxford University Press, Oxford, England, UK, 1961.

[12]Joseph, D. D., *Stability of Fluid Motion*, Springer-Verlag, Berlin FRG, 1976.

[13]Davis, S. H., "Buoyancy-Surface Tension Instability by the Method of Energy," *Journal of Fluid Mechanics*, Vol. 39, Part 2, 1969, pp. 347–359.

[14]Davis, S. H. and Homsy, G. M., "Energy Stability Theory for Free Surface Problems: Buoyancy-Thermocapillary Layers," *Journal of Fluid Mechanics*, Vol. 98, Part 3, 1980, pp. 527–553.

[15]Platten, J. K. and Legros, J. C., *Convection in Liquids*, Springer-Verlag, New York, 1984.

[16]Xu, Y., Zhang, N., and Yang, W.-J., "Direct-Recording Optical Methods for Visualizing Fluid Motion in Minute Liquid Bodies," in *Flow Visualization III*, edited by W.-J. Yang, Hemisphere, Washington, DC, 1985, pp. 668–672.

[17]Zhang, N. and Yang, W.-J., "Evaporation and Explosion of Drops on a Heated Surface," *Experiments in Fluids*, Vol. 1, No. 2, 1983, pp. 101–111.